



Investigation of the mycobacterial enzyme HsaD as a potential novel target for anti-tubercular agents using a fragment-based drug design approach

| | |
|-------------------------------|---|
| Journal: | <i>British Journal of Pharmacology</i> |
| Manuscript ID | Draft |
| Manuscript Type: | Research Paper Themed Issue |
| Date Submitted by the Author: | n/a |
| Complete List of Authors: | Ryan, Ali; Kingston University Faculty of Science Engineering and Computing polycarpou, elena; Kingston University London , Faculty of Science, Engineering and Computing Lack, Nathan; University of Oxford Department of Pharmacology; Koc Universitesi - Rumelifeneri Kampusu, School of Medicine Evangelopoulos, Dimitrios; University College London Centre for Clinical Microbiology; Birkbeck University of London Department of Biological Sciences; Francis Crick Institute, Mycobacterial Metabolism and Antibiotic Research Laboratory Sieg, Christian; Kingston University Faculty of Science Engineering and Computing Halman, Alice; Kingston University Faculty of Science Engineering and Computing Bhakta, Sanjib; Birkbeck University of London Department of Biological Sciences Eleftheriadou, Olga; Kingston University Faculty of Science Engineering and Computing McHugh, Timothy; University College London Centre for Clinical Microbiology Keany, Sebastian; University of Oxford Department of Pharmacology Lowe, Edward; University of Oxford Department of Biochemistry Ballet, Romain; University of Oxford Department of Pharmacology Abuhammad, Areej; University of Jordan, Department of Pharmaceutical Sciences Jacobs, William; Yeshiva University Albert Einstein College of Medicine, Department of Microbiology and Immunology, howard hughes medical institute Ciulli, Alessio ; University of Cambridge Department of Chemistry; University of Dundee College of Life Sciences Sim, Edith; University of Oxford Department of Pharmacology; Kingston University Faculty of Science Engineering and Computing |
| Major area of pharmacology: | Translational Pharmacology |
| Cross-cutting area: | Bacteria, Drug discovery/target validation |

| | |
|---------------------|--------------------------|
| Additional area(s): | Anti-microbials, Ligands |
| | |

SCHOLARONE™
Manuscripts

For Peer Review

Investigation of the mycobacterial enzyme HsaD as a potential novel target for anti-tubercular agents using a fragment-based drug design approach

Ali Ryan¹, Elena Polycarpou¹, Nathan Lack^{2,3}, Dimitrios Evangelopoulos^{4,5,6}, Christian Sieg¹, Alice Halman¹, Sanjib Bhakta⁴, Olga Eleftheriadou¹, Timothy D. McHugh⁵, Sebastian Keany², Edward D. Lowe⁷, Romain Ballet², Areej Abuhammad⁸, William R. Jacobs⁹, Alessio Ciulli^{10,11} and Edith Sim^{1,2*}

¹ Faculty of Science, Engineering and Computing, Kingston University London, Penrhyn Road, Kingston upon Thames, KT1 2EE, UK

² Department of Pharmacology, University of Oxford, Mansfield Road, Oxford, OX1 3QT, UK

³ Present address: School of Medicine, Koç University, Rumelifeneri Yolu, Sariyer, Istanbul, 34450, Turkey

⁴ Mycobacteria Research Laboratory, Institute of Structural and Molecular Biology, Department of Biological Sciences, Birkbeck, University of London, Malet Street, London WC1E 7HX, UK

⁵ Centre for Clinical Microbiology, University College London, Royal Free Campus, London, NW3 2PF, UK

⁶ Present address: Mycobacterial Metabolism and Antibiotic Research Laboratory, The Francis Crick Institute, Mill Hill Laboratory, London NW7 1AA, UK

⁷ Department of Biochemistry, University of Oxford, South Parks Road, Oxford, OX1 3QU, UK

⁸ School of Pharmacy, University of Jordan, Queen Rania Street, Amman 11942, Jordan

⁹ Department of Microbiology and Immunology, Howard Hughes Medical Institute, Albert Einstein College of Medicine, Bronx, New York, 10461, USA.

¹⁰ Department of Chemistry, University of Cambridge, Lensfield Road, Cambridge, CB2 1EW, UK

¹¹ Present address: Division of Biological Chemistry & Drug Discovery, School of Life Sciences, University of Dundee, James Black Centre, Dow Street, Dundee, DD1 5EH, UK

* Author to whom correspondence should be addressed: email edith.sim@pharm.ox.ac.uk

For Peer Review

Abstract

With the emergence of extensively drug-resistant tuberculosis there is a strong need for new anti-tubercular drugs that work through novel mechanisms of action. The *meta*-cleavage product hydrolase, HsaD, has been demonstrated in a genome-wide screen to be critical to the survival of *Mycobacterium tuberculosis* in macrophages and is encoded in an operon involved in cholesterol catabolism, which is identical in *M. tuberculosis* and *M. bovis* BCG. In this work we demonstrate that a strain of *M. bovis* BCG with a deletion of *hsaD* was unable to grow on cholesterol as a sole carbon source. Using a fragment based approach, over 1,000 compounds were screened by a combination of differential scanning fluorimetry, NMR spectroscopy and enzymatic assay with pure recombinant HsaD to identify potential inhibitors. Of seven chemically distinct “hits”, two chemical classes of fragments were pursued further using commercially available analogue sub-libraries. Following determination of inhibitory potency, the binding of inhibitors in the vicinity of the active site of HsaD was confirmed by determining the X-ray crystallographic structure of HsaD with individual fragments bound. The compounds were also tested for inhibition of growth of *M. tuberculosis* on cholesterol. The most potent inhibitor of HsaD was found also to be the best inhibitor of mycobacterial growth on cholesterol-supplemented minimal medium. We propose that HsaD is a novel therapeutic target which should be fully exploited in order to design and discover new anti-tubercular drugs.

Abbreviations: 4,9-DHSA, 4,5-9,10-diseco-3-hydroxy-5,9,17-trioxoandrosta-1(10), 2-diene-4-oic acid; ADC, albumin-dextrose-catalase; BCG, Bacillus Calmette–Guérin; CHES, N-Cyclohexyl-2-aminoethanesulfonic acid; DSF, differential scanning fluorimetry; FBDD, fragment based drug discovery; FCS, fetal calf serum; HOPDA, 2-hydroxy-6-oxo-6-phenylhexa-2,4-dienoic acid; LB, Luria-Bertani; MB, Middlebrook; MCP, *meta*-cleavage product; MDR-TB, multidrug-resistant tuberculosis; MIC, minimum inhibitory concentration; MTT, 3-(4,5-dimethylthiazol-2-yl)-2,5-diphenyltetrazolium bromide; NAT, arylamine N-acetyltransferase; OADC, oleic acid-albumin-dextrose-catalase; PMSF, phenylmethylsulfonyl fluoride; SAR, structure activity relationship; SPOTi, spot culture growth inhibition assay; STD, saturation transfer difference; TB, tuberculosis; TSP, (Trimethylsilyl)-propionic acid; WHO, World Health Organization; XDR-TB, extensively drug-resistant TB.

Introduction

Tuberculosis (TB) remains a global health emergency with an estimated 9 million new cases and 1.5 million deaths every year (WHO, 2015). Importantly, 3.7% of new cases and 20% of previously treated patients are infected with multidrug-resistant tuberculosis (MDR-TB). Moreover, up to 9% of these MDR-TB cases are resistant to nearly all known treatments and considered as extensively drug resistant TB (XDR-TB). Current treatment modalities for drug-sensitive TB cases require continuous dosing for at least six months of chemotherapy leading to poor patient compliance, which further increases the rate of drug resistance (WHO, 2015). There is a clear need for new anti-tubercular drugs, particularly those that shorten the treatment period. However the long-term and indefinite intracellular survival of *Mycobacterium tuberculosis* at different physiological states has made the development of novel therapeutics extremely challenging.

Cholesterol has been identified as important in the infection process of *M. tuberculosis* (Crowe *et al.*, 2015; Kendall *et al.*, 2007, 2010, Lloyd-Evans *et al.*, 2009; Lovewell *et al.*, 2016; Ouellet *et al.*, 2011; Peyron *et al.*, 2000) and is used as a carbon source during survival within macrophages (Pandey *et al.*, 2008; Rohde *et al.*, 2012). In previous work we have demonstrated that an operon consisting of *hsaA* (Rv3567), *hsaB* (Rv3570), *hsaC* (Rv3568), *hsaD* (Rv3569) (Van der Geize *et al.*, 2007) is involved in cholesterol metabolism. This operon was first identified in *M. tuberculosis* and also includes the gene encoding arylamine N-acetyltransferase (*nat*, Rv3566) (Anderton *et al.*, 2006; Payton *et al.*, 2001) and then further characterized in other mycobacterial species (Evangelopoulos *et al.*, 2014). It is currently believed that the NAT protein may metabolise the alkyl chain generated by cholesterol catabolism (Lack *et al.*, 2009), whilst the other proteins are involved in the degradation of the sterol nucleus of cholesterol (Van der Geize *et al.*, 2007; Griffin *et al.*, 2011; 2012). Studies using transposon mutagenesis have shown that HsaC and HsaD are required for the survival of *M. tuberculosis* within macrophages (Rengarajan *et al.*, 2005). The expression of *hsaC* gene was later demonstrated to be essential both *in vitro* and *in vivo* for infection of *M. tuberculosis* in guinea pigs (Yam *et al.*, 2009). More recent studies have also implicated a role for the operon and HsaD in mycobacterial growth linked to cholesterol catabolism (Griffin *et al.*, 2011). HsaD has also been shown to be overexpressed in hypervirulent strains of *Mycobacterium bovis* BCG during mouse infection (Blanco *et al.* 2009) and compounds with antitubercular activity have been identified as potential HsaD inhibitors via virtual screening (Rebollo-Lopez *et al.*, 2015).

HsaD belongs to the superfamily of $\alpha\beta$ -hydrolases that consists of the *meta*-cleavage product (MCP) hydrolase subfamily (Lack *et al.*, 2008). HsaD catalyses the hydrolytic cleavage of the carbon-carbon bond, through a serine protease-like catalytic triad (Lack *et al.*, 2008; Lack *et al.*, 2010), of the MCP 4,5-9,10-diseco-3-hydroxy-5,9,17-trioxoandrosta-1(10),2-diene-4-oic acid (4,9-DHSA) in the cholesterol metabolism pathway (Van der Geize *et al.*, 2007). In a previous study, we demonstrated that mechanism-based serine protease inhibitors can inhibit HsaD (Ryan *et al.*, 2014) suggesting that an acyl enzyme intermediate may be formed during the reaction process in line with studies on the mechanism of other C-C bond hydrolases (Ruzzini *et al.*, 2012;2013). As the HsaC protein (Yam *et al.*, 2009) is unstable in oxygen, HsaD is a promising pharmacological target essential for *M. tuberculosis* infection. It is highly soluble as a stable recombinant protein (Lack *et al.*, 2009) and there are multiple crystal structures available (Lack *et al.*, 2008; Lack *et al.*, 2010). Moreover HsaD has a very large active site cavity that makes it a good target for fragment based drug discovery (FBDD) (Silvestre *et al.*, 2013). FBDD combines NMR, differential scanning fluorimetry (DSF) and crystallography to use weakly binding small molecules (<300Da) as building blocks to develop potent small molecular inhibitors. This approach has shown tremendous success in modern drug discovery (Hudson *et al.*, 2012; Hung *et al.*, 2016).

In this study we investigate HsaD as a novel pharmacological target for tuberculosis through generation of a specific gene deletion mutant and describe the identification of compounds as inhibitors of HsaD by a FBDD approach.

Materials and methods

All reagents were purchased from Sigma Aldrich (Poole, UK) unless otherwise stated. 3,5-dichlorobenzenesulphonamide, 3-chloro-4-hydroxybenzoate and 4-toluenesulphonamide were obtained from TCI Europe. 3,5-difluorobenzenesulphonamide, 3,5-dichlorobenzamide and 3-bromobenzenesulphonamide were obtained from Apollo Scientific and ethyl-3,5-dichloro-4-hydroxybenzoate was obtained from Maybridge. The fragment library used in this study was composed of 1258 compounds from commercial libraries supplied by Maybridge (Thermo Fisher Scientific: <http://www.maybridge.com/>), as previously described (Ciulli,

2013; Van Molle *et al.*, 2012). All library compounds were dissolved and stored in d_6 -DMSO.

All inhibitors were dissolved in DMSO. The DMSO final concentration in the assays was 5% (v/v) for the enzymatic assays and between 0.02% and 1.7% (v/v) for the growth experiments. The synthetic substrate, 2-hydroxy-6-oxo-6-phenylhexa-2,4-dienoic acid (HOPDA) was synthesised by Almac Sciences (Craigavon, Northern Ireland) as previously described and dissolved in ethanol (1% v/v) (Lack *et al.*, 2009). The fragment library was prepared as previously described (Ciulli, 2013; Van Molle *et al.*, 2012).

Bacterial growth conditions

M. tuberculosis, *M. bovis* BCG and *Mycobacterium smegmatis* mc²155 liquid cultures were grown in Middlebrook (MB) 7H9 broth containing 10% (v/v) ADC (albumin-dextrose-catalase), 0.2% (v/v) glycerol and 0.05% (v/v) Tween-80. Mycobacterial strains were also grown on MB7H10 agar containing 10% (v/v) OADC (oleic acid-albumin-dextrose-catalase) and 0.5% (v/v) glycerol. *M. tuberculosis* cultures were grown in 10 mL broth in a 30 mL vials as standing cultures, *M. bovis* BCG in 100 mL broth in a roller bottle rolling cultures at 2 rpm and *M. smegmatis* in 10 mL in a 50 mL centrifuge tubes rotating at 180 rpm all in a 37°C incubator, unless specified otherwise. Δ *hsaD* *M. bovis* BCG was further supplemented with 50 µg/mL hygromycin.

Growth curve comparison of the wild-type and Δ *hsaD* *M. bovis* BCG were done in minimal medium containing 0.05% (v/v) tyloxapol and 0.05% (v/v) ethanol with either a) no additional carbon source, b) 100 µg/mL glycerol or, c) 100 µg/mL cholesterol. An equivalent number of bacteria (6×10^8) were added to start the cultures and the bacterial growth rate was measured by monitoring the OD₆₀₀ daily for 16 days.

E. coli JM109 cells were grown in Luria-Bertani (LB) broth 10 mL of a centrifuge tube rotating at 180 rpm a 37°C incubator. LB agar was used for solid growth of *E. coli* strains at 37°C, unless specified otherwise.

Generation of the Δ *hsaD* gene deletion

Deletion of the *hsaD* gene was performed using specialised transduction as previously described (Bardarov *et al.*, 2002). Briefly, the upstream and downstream flanking DNA regions of the *hsaD* gene were amplified by PCR using the following pair of oligonucleotide primers for the upstream flanking DNA region 5'-TTTTTTTTGCATAAATTGCAGGCACCGTAGGCCAT-3' and 5'-TTTTTTTTGCATTTCTTGCAGTGACGTCCATTCAACA-3' as the forward and reverse primers respectively with a *Bst*API restriction site (underlined). The primers for the downstream flanking region were 5'-TTTTTTTTCACAGAGTGCTTGACCGAGGCAATTGGAGAC-3' and 5'-TTTTTTTTCACCTTGTCACCTGTTGGGCGGGC-3' as the forward right and reverse primers respectively with a *Dra*III restriction site (underlined). The upstream and downstream products were subsequently digested with *Dra*III and *Bst*API, respectively, and ligated with *Pf*MI-digested p0004s vector arms. The knockout construct was linearised following digestion with *Pac*I and cloned into phAE159. Both pAES and phAE159 were subsequently digested with *Pac*I, gel purified and ligated with T4 DNA ligase. The ligation mixture was then packaged into λ phage heads by *in vitro* packaging, transduced into *E. coli* and plated on LB agar supplemented with hygromycin. Following validation the phasmids were then electroporated into *M. smegmatis* and grown at a permissive temperature (30°C) to generate mycobacteriophages. The resulting high-titre mycobacteriophages were then used to transduce the recipient mycobacteria at 37°C (non-permissive temperature). The correct identity of loss-of-function mutations was confirmed by PCR amplifications with primers against the internal *hsaD* gene (forward: 5' AAGTCGGCTCCGGC 3' reverse: 5' TGGCCGTCGACCAGC 3') and the region flanking the *hsaD* deletion (forward: 5' GATGCTCATCTGCCACC 3' reverse: 5' ATGACAGCTACCGAGGAAT 3').

Intracellular survival of Δ *hsaD* *M. bovis* BCG in macrophages

The RAW264.7 mouse macrophage cells were grown as a monolayer in RPMI-1640 media (GIBCO, Paisley, UK), supplemented with 1% (w/v) L-glutamine and 10% (v/v) foetal calf serum (FCS) at 37°C with 5% CO₂. For the intracellular survival assays, RAW264.7 cells were plated approximately 24 hours prior to infection on 6-well plates in the presence of 2 mL RPMI (supplemented with 10% FCS) as described (Bhakta *et al.*, 2004; Westwood *et al.*, 2010). Cells were subsequently washed with fresh media, infected with *M. bovis* BCG at a

multiplicity of infection of 20 (i.e for every 1 RAW264.7 cell, 20 cells of *M. bovis* BCG were added) and incubated for 2 h. Cells were then washed twice with PBS and re-suspended in fresh media. The media was later removed and the cells were lysed with 1 mL of sterile distilled water for 10 min at 0, 24, 48, 72 and 120 h. The number of intracellular bacteria was determined by serially diluting the lysate, plating it on MB7H10 agar plates and incubating at 37°C for 3-4 weeks.

Effect of inhibitors against *M. tuberculosis* grown in cholesterol

Growth on agar was carried out as follows: The minimum inhibitory concentrations (MIC) of selected inhibitors were determined using the spot culture growth inhibition assay (SPOTi) performed in 24-well plates with slight modifications (Evangelopoulos & Bhakta., 2010). Briefly, mycobacteria were plated on minimal agar based media containing: asparagine (0.5 g/L), KH_2PO_4 (1.0 g/L), Na_2HPO_4 (2.5 g/L), ferric ammonium citrate (50 mg/L), $\text{MgSO}_4 \cdot 7\text{H}_2\text{O}$ (0.5 g/L), CaCl_2 (0.5 mg/L), ZnSO_4 (0.1 mg/L), agar (1.5% w/v) and either glycerol (0.1% v/v) or cholesterol (0.01% w/v). Fragments dissolved in DMSO (0.0125 $\mu\text{g/mL}$, 0.025 $\mu\text{g/mL}$, 0.05 $\mu\text{g/mL}$, 0.1 $\mu\text{g/mL}$, and 0.2 $\mu\text{g/mL}$) or DMSO alone were mixed with 2 mL of the minimal media with cholesterol per well. The final DMSO concentration in the wells containing fragments was 0.2%. In addition a well with 0.2% DMSO only as well as isoniazid at various concentrations (0.001 $\mu\text{g/mL}$, 0.01 $\mu\text{g/mL}$, 0.1 $\mu\text{g/mL}$, 1 $\mu\text{g/mL}$ and 10 $\mu\text{g/mL}$) were used as positive controls. The plates were then inoculated with 2 μL (approximately 10^3 viable cells) of a mid-log phase culture of either *M. bovis* BCG or *M. tuberculosis* that was added in the centre of each well and allowed to soak before the plates were sealed with para-film, wrapped with aluminium foil and incubated at 37°C for 2 weeks until a spot of colonies were developed in the control wells. The MIC was determined as the lowest concentration in the well where mycobacterial growth was not evident.

Effect of inhibitors against *E. coli*

An overnight culture of *E. coli* JM109 cells grown as stated before was diluted in LB media to a final OD_{600} of 0.1 and acted as a working culture. 10 μL of this working culture was used to inoculate a 96 well plate containing 90 μL of LB media with a range of inhibitor concentrations up to 100 $\mu\text{g/mL}$. The maximum DMSO concentration in the well was 1.7% (v/v). The plates were then transferred into the Tecan M200 Infinite Pro spectrophotometer

where they grew at 37°C as standing cultures with absorbance measurements at 600nm taken every hour for 4 hours

Cytotoxicity against mammalian cells

Cytotoxicity was tested using CCL-228 colorectal cancer cells (American Tissue Culture Collection Manassas, VA). Cells were cultured in Dulbecco's Minimum Essential Medium (GIBCO, UK), supplemented with 10% (v/v) foetal bovine serum (FBS; Sigma-Aldrich, Poole, UK), 10,000U penicillin, 10 mg/mL streptomycin in 0.9% NaCl (Sigma-Aldrich), and maintained at 37°C in a humidified atmosphere with 5% CO₂. Cells were seeded in 96-well plates (20,000 cells/well) and treated for 48 h after which they were incubated with 100µL of 50µg/mL MTT solution in phenol red free DMEM (GIBCO) for 3 h in the dark at 37°C. The MTT was removed and the crystals solubilised with 100µL DMSO for 15 min at room temperature with gentle shaking. The intensity was measured colorimetrically at 570 nm using the M200 Infinite Pro plate reader (Tecan) and percent growth was calculated.

Fragment based drug discovery

Recombinant HsaD was prepared as described previously (Lack et al 2009). Differential scanning fluorimetry (DSF) was performed on a total of 1258 fragments as described previously (Niesen *et al.*, 2007), using 0.4-1 µM HsaD in the presence of 2.5× SYPRO orange (Invitrogen) and 2.5 mM of compound (0.5 µL from a 0.1 M stock) at a final volume of 100 µL per well (final DMSO concentration of 2.5%) in 50 mM HEPES 300 mM NaCl pH 7.5. Fluorescence was monitored using an Agilent Mx3005p qPCR instrument (Santa Clara, USA). The fluorescence excitation and emission wavelengths were 483 and 533 nm. The output data was plotted as derivative of the fluorescence versus temperature, and the maximum of such derivative over temperature was determined as the melting temperature (T_M). Hits from the primary DSF screen were identified by the shift in T_M compared to HsaD with vehicle (>2× st. dev. of control samples) and were further re-tested twice to confirm the results.

NMR fragment screening

Confirmed hits were validated by ligand-observed NMR spectroscopy (Ciulli & Abell, 2007; Ciulli, 2013; Dalvit *et al.*, 2001; Ferguson *et al.*, 2013). All NMR experiments were carried out at 278 K on a Bruker Avance 700 MHz equipped with a 5 mm triple TXI cryoprobe with *z* gradients. Relaxation-edited NMR experiments incorporated a CPMG spin-lock time of

200 ms before the acquisition period (Carr & Purcell, 1954). . Saturation Transfer Difference (STD) NMR experiments employed a 40 ms selective Gaussian 180° shaped pulse at a frequency alternating between ‘on resonance’ (0.5 ppm) and ‘off resonance’ (~80 ppm) after every scan (Mayer & Meyer, 1999). Water suppression was achieved by using a W5 Watergate gradient spin-echo pulse sequence (Piotto et al., 1992). WaterLOGSY experiments (Dalvit *et al.*, 2000;2001) employed a 20 ms selective Gaussian 180° shaped pulse at the water frequency and an NOE mixing time of 1 s. Water suppression was achieved using a double-gradient echo excitation sculpting sequence with gradients. The resulting spectra were analyzed using Topspin 2.0 software (Bruker). All samples were made up to a total volume of 200 µL in 3 mm capillaries, and contained 1.2 mM fragment, 50 mM Tris-HCl buffer at pH 7.5, 10% v/v D₂O, and 2.4% v/v DMSO-*d*₆. (Trimethylsilyl)-propionic acid-*d*₄ (TSP) was present at 20 µM concentration in all samples for calibration purposes. A protein only control sample was run as buffer control. Each fragment was run as 3 samples – (A-C). A) Fragment only; B) Fragment + protein (10 µM HsaD); C) Fragment +HsaD + displacer compound PMSF (100 µM).

Enzymatic assays

Following the initial identification of fragments from the fragment based drug design library, inhibition assays were carried out as previously described (Ryan et al., 2014) in the presence of 1 mM with compounds 1-7. Subsequently, compounds that were capable of inhibiting the cleavage of HOPDA by HsaD, were further selected for IC₅₀ determination using a range of concentrations (1 mM, 0.5 mM, 0.375 mM, 0.25 mM, 0.125 mM, 0.05 mM and 0 mM or 3.5 mM, 3 mM, 2.5 mM, 2 mM, 1.5 mM, 1 mM, 0.5 mM and 0 mM). Briefly pure HsaD (16 µg/mL in 100 mM phosphate buffer pH 7.5, 20 mM NaCl) was added to the reaction mixture in the presence of 100 µM HOPDA (final concentration of 1% ethanol v/v) and inhibitor (final DMSO concentration of 5%) in a final volume of 100 µL. The enzymatic activity was measured by monitoring the absorbance at 450 nm at 21°C using a M200 Infinite Pro plate reader (Tecan) and the IC₅₀ was determined using GraphPad Prism. The ε₄₅₀ of HOPDA was measured as 13,200 M⁻¹cm⁻¹.

Solution of the structures of HsaD with Fragments 2, 27 and 32

Crystals of apo-HsaD were grown as described previously (Lack *et al.*, 2008). All fragments were dissolved directly into the cryoprotectant containing 30 % (w/v) PEG-3000, 0.1 M CHES pH 9.5, 25% (v/v) glycerol, at concentrations of between 15 mM and 50 mM. Crystals were transferred into the cryoprotectant containing one of the fragments and allowed to soak overnight at 21°C before flash freezing for analysis.

Data collection for the structures of HsaD bound to **2**, **27** and **32** were all performed at the Diamond Light source (Oxon, UK) using beamline I24 in the case of the structure with **2** and using beamline I03 for the others. In all cases initial processing was performed via Xia2 (Winter, 2010) using XDS (Kabsch, 2010) to index and either Scala (**2**) (Evans, 2006) or Aimless (Collaborative Computational Project, 1994) (Winn *et al.*, 2011) (**27** and **32**), to merge and scale the data. The structure was solved via molecular replacement using PHASER (McCoy *et al.*, 2007) using the structure of apo-HsaD (PDB code, 2vf2) (Lack *et al.*, 2008) stripped of all ligands as a search model. The atomic models were rebuilt in COOT (Emsley *et al.*, 2010) and refined using REFMAC (Murshudov *et al.*, 1997) and PHENIX (Adams *et al.*, 2010). Model restraints for **2**, **27** and **32** were generated in eLBOW (Moriarty *et al.*, 2009).

Results and Discussion

Growth

Deletion of *hsaD* in *M. bovis* BCG (Δ *hsaD*) was generated using a mycobacteriophage-based knockout method (Bardarov *et al.*, 2002). All of the hygromycin resistant colonies tested were the correct mutant. Our results are in accordance with previous studies, which have reported that approximately 95% of antibiotic-resistant transductants were the correct genotype (Bardarov *et al.*, 2002).

When grown in MB7H9 broth (Figure 1A) or in minimal medium (Figure 1B) the deletion of *hsaD* had no apparent effect on bacterial growth when compared with *M. bovis* BCG. However, when the minimal medium was supplemented with cholesterol (Figure 1C), a significant difference between the two strains was observed. Whilst the growth of the wild type strain was very similar to that in minimal medium alone, the growth of Δ *hsaD* *M. bovis*

BCG was significantly inhibited in the presence of cholesterol as compared to *M. bovis* BCG (Figures 1B & C). The growth of Δ *hsaD* *M. bovis* BCG in the presence of cholesterol was suppressed compared with growth in minimal medium alone. It has been observed that when the Δ *hsaC* *M. tuberculosis* H37Rv strain is grown in minimal medium with cholesterol there is a change in the appearance of liquid cultures such that they develop a pink colour (Yam *et al.*, 2009). We observed the same effect when *hsaD* is deleted from *M. smegmatis* (Supplementary Figure 1) and grown on cholesterol as carbon source. Therefore, similar to the “pink” metabolite of the Δ *hsaC* *M. tuberculosis* we propose that deletion of *hsaD* results in inhibition of growth of *M. bovis* BCG on cholesterol as a result of accumulation of an inhibitory metabolite. Growth in minimal medium on glycerol as the sole carbon source is supported in both the Δ *hsaD* strain and *M. bovis* BCG. The gene deleted strain showed a slight lag in rate of growth although it caught up by day 16, reaching the same optical density ($OD_{600} = 1.5$) (Figure 1D). These data mirror previous findings on deletion of *hsaD* and other essential genes involved in cholesterol catabolism from *M. tuberculosis* (Griffin *et al.*, 2011). Additionally it has been observed that *hsaD* expression is significantly increased in *M. smegmatis* when grown on cholesterol (Uhiá *et al.*, 2012) and genome wide studies with *M. smegmatis* grown on cholesterol have also pointed to an essential role for (Li *et al.*, 2016).

Growth in minimal medium on glycerol as the sole carbon source is supported in both the Δ *hsaD* strain and *M. bovis* BCG. The gene deleted strain showed a slight lag in rate of growth although it caught up by day 16, reaching the same optical density ($OD_{600} = 1.5$) (Figure 1D). These data mirror previous findings on deletion of *hsaD* and other essential genes involved in cholesterol catabolism from *M. tuberculosis* (Griffin *et al.*, 2011).

Whole genome studies have previously identified the role of HsaD in the survival of *M. tuberculosis* within macrophages (Sasseti *et al.*, 2003; Griffin *et al.*, 2011). It has also been demonstrated that other genes in the operon (*hsaC* and *nat*) are essential for survival of *M. bovis* BCG in macrophage (Anderton *et al.*, 2006; Bhakta *et al.*, 2004). We therefore investigated the intracellular survival of the wildtype and Δ *hsaD* strains of *M. bovis* BCG within RAW246.7 mouse macrophages. Similar to Δ *hsaC* and Δ *nat* strains, there was a reduction in intracellular growth of the Δ *hsaD* strain as compared to the *M. bovis* BCG (Figure 1E). This is consistent with the whole genome studies and studies identifying the role of other members of this operon in the metabolism of cholesterol, which has been identified as controlled as the *Kst*-Regulon (Kendall *et al.*, 2007; Uhiá *et al.*, 2012)).

Identification of chemical fragments as inhibitors of HsaD

The studies described above add to the growing weight of evidence that the operon in which *hsaD* is encoded along with the *nat* gene in the same gene cluster (Anderton *et al.*, 2006) are essential for intracellular survival of mycobacteria and also that the gene product are required for cholesterol metabolism in *M. bovis* BCG and *M. tuberculosis* (Kendall *et al.*, 2010; Van der Geize *et al.*, 2007; Yam *et al.*, 2009). Given this importance, we speculated that the *hsaD* gene is a potential target for anti-tubercular agents. Supporting drug design, the crystal structure of HsaD has been established to better than 2 Å resolution with the substrate HOPDA bound and shows that the active site cleft is over 30 Å³, which is a good prospect for a fragment based approach to identifying inhibitors (Lack *et al.*, 2010). HsaD is also a stable soluble protein which crystallises readily (Ryan *et al.*, 2014). Moreover, chemical inhibitors of HsaAB were found to dramatically decrease the intracellular proliferation of *M. tuberculosis* in macrophages (VanderVen *et al.*, 2015).

A commercial library of rule-of-three compliant 1258 fragments (Silvestre *et al.*, 2013) was screened by DSF. The melting temperature of pure recombinant HsaD was monitored in the presence of the fragments. The melting temperature of HsaD in previous studies (Lack *et al.*, 2009) had been determined by circular dichroism and loss of enzymatic activity of the protein itself to be between 69 and 72 °C. The high melting temperature was confirmed by DSF monitored by SYPRO Orange to be 72.7 (average mean value from quadruplicates across 17 plates) +/- 0.21 °C (average SD from quadruplicates across 17 plates) in the presence of solvent and no added fragment. Fragments were identified as potential binders to purified HsaD when a shift was monitored in the melting temperature of greater than two standard deviations from the mean melting temperature of pure HsaD alone (Table 1). Hit compounds (18) from the primary screen were re-tested in duplicates in the thermal shift assay, from which 8 confirmed. The validated fragments were also tested as inhibitors of HsaD at a concentration of 1 mM of the compound (Figure 2) and were in addition tested by saturation transfer NMR for displacement by PMSF, an already identified inhibitor (Ryan *et al.*, 2014) (Table 1 & Figure 2A).

From this combination of methods, a series of seven distinct fragments were identified as binders. Fragment 1 was not pursued further due to its insolubility at 1 mM. In addition to the “hits” from the screen, a selection of 20 compounds from the library which showed no

evidence of binding by the DSF criteria, were also tested at 1 mM as inhibitors of HsaD and none were found to inhibit the enzyme (Data not shown). From the initial inhibition studies at 1 mM, two compounds looked promising - compound **2** and compound **6**, which produced 38 % and 60% inhibition respectively (Figure 2). Fragment **2** is a sulphonamide and fragment **6** is a hydroxybenzoate.

When tested at a range of concentrations, compound **2** (3,5-dichlorobenzenesulfonamide) is an inhibitor of HsaD with an IC_{50} of 0.43 mM (Table 2) and fragment **6** (ethyl 3,5-dichloro-4-hydroxybenzoate), despite it not being displaced by PMSF (Table 1), is also an inhibitor of HsaD with an IC_{50} of 0.55 mM (Table 2).

The fragments which were identified were distinct from previously identified substrates (Lack *et al.*, 2010) and also distinct from putative inhibitors identified from a virtual screen (Rebollo-Lopez *et al.*, 2015) but interestingly bear some resemblance to the central moiety of an inhibitor identified as targeting the HsaAB protein complex of the same operon (Vanderven *et al.*, 2015).

A small series of compounds related to each of the two classes of hit fragments **2** and **6** was tested for inhibition of HsaD (Supplementary table 1).

Derivatives of fragment 2 as inhibitors of HsaD

We investigated the small series of fragments modified around Compound **2** which has two chlorine atoms at the *meta* position. We investigated the effects of altering the position and number of chlorines in the molecule as well as substituting different halide groups. Removal of one chlorine from position 3 (Compound **9**) was detrimental to the inhibitory potency and the IC_{50} was increased more than 10 fold to 5.14 mM (Supplementary table 1). Removal of both the chlorine atoms as in compound **8** (Supplementary Table 1 & Table 2), destroyed inhibition of HsaD completely. Substitution of the chlorines by fluorine (Fragment **10**) also resulted in loss of inhibition of HsaD (Supplementary Table 1). Having a single chlorine in the *para* position (Fragment **13**) did not possess any inhibitory effects on HsaD (Supplementary Table 1).

Altering the position of chlorine from *meta* to the *ortho* position (Fragment **11**) likewise resulted in a decreased inhibitory effect (IC_{50} 1.96 mM) compared with fragment **2** and changing the chlorines to trifluoromethyl compounds (fragment **12**) showed poorer inhibition as compared to the initial compound with less than 50% inhibition being reached.

(Supplementary Table 1). Mono-substituted benzenesulfonamides with a bromine in position 3 (Fragment **14**), like the mono-chlorinated fragment, produced a similar IC_{50} of 2.74 mM.

The library of fragments used for these studies also incorporated sulphonamide fragments with the addition of nitro-, amino-, methyl-, methoxy-, hydroxy-, and carboxy- groups on various positions of the benzene ring. None of the modifications including these side groups were capable of inhibiting HsaD (Fragments **15-23**) with the exception of Fragment **20** which, with an IC_{50} of 92.6 mM, was an extremely poor inhibitor.

A derivative of Fragment **2**, 3,5-dichlorosulfanilamide in which an amide group was incorporated in position 4 of the benzene ring, was able to inhibit HsaD with an IC_{50} of 0.184 mM (Fragment **24**) (Table 2 and Supplementary Table 1). Addition of a dimethyl group on the nitrogen (Fragment **25**), however reduced the inhibitory effect on HsaD with an IC_{50} of 3.63 mM. Replacement of the chlorines with bromines (Fragment **26**) reduced the inhibitory potency compared with the parent compound to IC_{50} 2.16 mM.

The important features for inhibition of HsaD by derivatives of **2** appear to be a *para* hydroxyl group on the aromatic ring and two chlorines as *meta* substituents and the inhibitory potency (IC_{50} of 0.27mM) of fragment 27 supports this conclusion. Fragment 27 also has a sulfonate group at position 1 (Table 2).

Derivatives of compound 6 as inhibitors of HsaD

A small group of hydroxybenzoate analogues were tested for comparison with compound **6** as inhibitors of HsaD.

Like compound **2**, compound **6** has *meta* (3,5) substituted chlorine atoms and the position and number of chlorine substituents on the aromatic ring was altered as well as the presence of the 4-hydroxyl group.

Ethyl 3,5-dichloro-4-hydroxybenzoate (Fragment **6**) inhibited HsaD (IC_{50} 0.55 mM). When the hydroxyl group was removed there was no inhibition of HsaD (Fragment **28**) and when either one or both of the chlorine atoms were removed no inhibition was then observed. Fragment **29** with only one chlorine at the 3 position was not inhibitory and the same was true when both chlorines were missing (Compound **30**).

An analogue in which both the chlorines are present and the 4 hydroxyl is present but there is a change in the ester substituent on the 1 position to a carboxylate group (3,5-dichloro-4-hydroxybenzoic acid - Fragment **32**) has the same IC_{50} value of 0.54 mM as the parent compound (Table 2B and Supplementary table 1). If the hydroxyl group in this charged compound is substituted by an amino group (fragment **33**), the IC_{50} remains the same (0.54 mM). Interestingly, altering the ethyl substituent on the carboxylate group to a methyl group (compound **31**) was inhibitory but with a slightly higher IC_{50} (0.73 mM).

To further elucidate the importance of the chlorines on positions 3 and 5, these were rearranged into positions 1 and 3 with the addition of a nitro group in position 6 (Fragment **35**). The resulting compound was less inhibitory, with an IC_{50} of 2.14 mM. Removal of the chlorines and only the presence of the carboxylic acid and amine group in positions 1 and 4 of the benzene ring respectively (Fragment **36**) and the amine in position 3 (Fragment **37**), completely reversed the inhibitory effect (Supplementary Table 1).

These studies supported the conclusion that the presence of chlorine substituents on the ring at the *meta* positions and the presence of a hydroxyl at the *para* position are important features for inhibition of HsaD.

Structural studies of HsaD with inhibitors

In order to identify the mode of binding of the inhibitors which were identified, structural studies were carried out using three different inhibitors : Compound **2** (IC_{50} , 0.55mM) and an analogue (compound **27**, IC_{50} , 0.27mM) were chosen as representatives of the sulphonamide series and compound **32** (IC_{50} , 0.54mM) was chosen as a representative of the hydroxybenzoate class. The latter compound was chosen in preference to the parent compound because it is more soluble. Crystals of HsaD were soaked with the inhibitory fragments.

The structure of HsaD has been determined alone (Lack *et al.*, 2008) to 2.6 Å and the structure of an inactive S114A mutant of HsaD has been determined at resolutions of better than 2 Å with one of several different substrates bound (Lack *et al.*, 2010). It was necessary to use the inactive version of HsaD in order for the substrate/protein complex to be stable enough for crystallisation. In each of the crystal structures, the asymmetric unit consists of 2 protomers of identical polypeptide chains with one protomer being assigned as the A chain and the other as the B chain. These protomers are identical and each folds to form an α/β

hydrolase fold which contains an active site including the catalytic triad (Ser114, His269 and Asp 241). (Lack *et al.*, 2008; Lack *et al.*, 2010).

The crystal structure of HsaD with compound 2, was obtained to a resolution of 2.1 Å. The crystal structure with 3,5-dichloro-4-hydroxybenzenesulphonic acid (fragment 27) was obtained at a resolution of 2.68 Å and the structure of HsaD was also obtained where the ligand bound was a derivative of hydroxybenzoic acid (3,5-dichloro-4-hydroxybenzoic acid Fragment 32), at a resolution of 2.27 Å.

The crystal structures of each of these ligand bound structures can be compared with the structure of HsaD alone (Figure 3A). With the exception of a 55° rotation of the side chain of Trp270, which is only observed in the structure of HsaD with compound 2, there are no major conformational changes compared with structure of apo-HsaD (overall RMSD 0.2 - Figure 3). The binding of substrate molecules to HsaD revealed the presence of two different conformations, an open conformation for the apo-enzyme and a closed conformation when the substrate was bound. However, there was no change in the juxtaposition of the active site residues in the main catalytic pocket. The same is true on the binding of the inhibitors which have been investigated here (Figure 3A).

Two molecules of fragments 2 and 27 were observed bound to HsaD, in their respective structures: one molecule was bound in each of the active sites of the protomers in the dimer in the asymmetric unit. In each of these cases the orientation of the ligand was superimposable in its orientation in each of the two active sites in the dimer.

Compound 32 was found in only one of the active sites of the dimer in the asymmetric unit, with the A chain active site being unoccupied. This reflects the data obtained with the substrate bound structures (Lack *et al.*, 2010). The inhibitor binding sites each overlap with the binding site of the substrate from previous structures (Figure 4D) and are close to the active site Ser (Fig 3B-D). These structural studies confirm the specificity of the screening process in identifying inhibitors of HsaD.

Binding of 2 and its analogue 27 to HsaD

The structure of HsaD bound to fragment 2 allowed the unambiguous determination of the fragment's binding orientation. Fragment 2 binds within the active site with its sulphonamide group making short-range hydrogen bonds with the side chain of Asn244 (Figure 3B). It also forms a hydrogen bond with the backbone amide of Gly140 and a water bridged interaction

with the side chain of Asn89. The benzene ring forms hydrophobic contacts with Gly46 and the side chains of Leu115, Leu158 and Val243. One chlorine forms contacts with the side chains of Met208 and Phe220, while the other contacts the side chains of Phe173 and His269.

The number of hydrophobic contacts made by the chlorines explains why removal of one or both has a detrimental effect on fragment binding (Fragments **8** and **9**) and also why replacement of the chlorines with polar functional groups is energetically unfavourable (Fragments **16**, **18**, **20**). The importance of the interactions of chlorines at positions 3 and 5 also explains the inability of **17**, **21** and **22** to inhibit HsaD. The hydrophobic contacts with Met208 and Phe220 are relatively long range (4.3 Å and 4.8 Å respectively) which indicates why the bromine of the inhibitory fragment **14** could be accommodated.

The short-range hydrogen bond formed by the sulphonamide nitrogen explains the detrimental effect observed by double methylation of this group in fragment **25**. Accommodation of the sulphanilamide of **24** in the current orientation would not be possible due to the distance between the fragment's ring and Gly46 being too short to allow accommodation of an amine group in between (3.7 Å).

Fragment **27** binds with its acidic group at the entrance of the polar sub-pocket (Fig 3C) that binds the dienoate moieties of HOPDA and 4,9-DHSA (Lack *et al.*, 2010). The sulphonate group of **27** forms hydrogen bonds with the side chain of Trp270 as well as the backbone amides of Gly45 and Gly46 (Figure 3C). The sulphonate also forms a salt bridge interaction with the side chain of Arg192 (4.5 Å). One of the chlorines of **27** fits into a hydrophobic pocket formed by the side chains of Leu158, Phe173, Met177 and Val243 (all distances <4Å). The other chlorine interacts with Gly45 and the side chain of Leu115.

The acidic compound **27**, binds in a different orientation to the uncharged sulphonamide **2** (Figure 4B). The charged sulphonate group of **27** may drive its binding to the polar pocket of the active site where it is able to form the salt bridge with Arg192 that could not be formed with the neutral sulphonamide of **2**. This clear distinction in the binding modes of fragments that have charged versus simply polar groups provides useful information for modifying the fragments to improve affinity.

Binding of fragment 32 to HsaD

Fragment **32** binds in an almost coplanar conformation to **27** (Figure 3D). However, its binding position is shifted by around 1.8 Å outward from the polar sub-site (Figure 4A). As a

result, the carboxyl group of **32** is not inserted as far into the pocket as the sulphonate of **27**. The carboxyl group forms hydrogen bonds with the side chain of Ser114 and the backbone amides of Gly45 and Gly46 (Figure 3D). This also means the fragment is unlikely to form a salt bridge with Arg192 (separation $>6 \text{ \AA}$). The altered binding conformation also removes the interaction of the chlorine with Gly45, leaving only the contact with Leu115. The other chlorine still contacts Leu158, Phe173 and Val243 but does not contact Met177, rather, it interacts with Val155.

The extensive hydrophobic contacts made by both chlorines of **32**, explains their importance in the binding of the fragment. In view of the proposed importance for the 4-hydroxy group of **32** in the inhibition of HsaD, it was unexpected to find the hydroxyl group makes no interactions with either the side chain or backbone of HsaD.

The binding of **32** (Figure 3D), like the other acidic inhibitor investigated (**27** Figure 3C) shows a distinct binding orientation from the uncharged sulphonamide (fragment **2**) Figure 4.

From these comparisons of binding sites, using fragment **2** as a starting point (Figure 4) there are two possible areas of expansion, the first is into the polar pocket that is accessed by the acidic groups of **27** and **32** (Figure 4C). The second area of expansion would be into the strongly negatively pocket in close proximity to the sulphonamide group of **2**. Expansion into this polar pocket would mimic that of HOPDA (Figure 4D) which extends deep into the pocket and makes shorter range salt bridge with Arg192 (3.1 \AA).

Effects of inhibitors on growth of *M. bovis* BCG and *M. tuberculosis* H37Rv.

In order to evaluate the specific anti-mycobacterial activity of the compounds, we tested them for inhibition of growth against *E. coli*. There was no inhibition observed at up to $100 \mu\text{g/mL}$ (Supplementary Figure 2). We also tested for any cytotoxic effect against RAW264.7 murine macrophage cells and again found no evidence of eukaryotic cell toxicity at concentrations up to $100 \mu\text{g/mL}$ (data not shown).

None of the HsaD inhibitors had any effect on the growth of *M. bovis* BCG or *M. tuberculosis* when cultured in enriched MB7H9 broth. This observation is consistent with the effect seen in the gene deleted mutant strains. In order to test the proof of principle that inhibitors of HsaD would have an effect on the growth of *M bovis* BCG and *M. tuberculosis*

on cholesterol, we tested the fragments at concentrations ranging from 12.5 $\mu\text{g}/\text{mL}$ to 200 $\mu\text{g}/\text{mL}$ in minimal growth media supplemented with cholesterol, using the SPOTi assay. Fragment **6** which is one of the most potent inhibitors of HsaD was also the most effective at inhibiting growth of both *M. bovis* BCG and *M. tuberculosis* treatment in the presence of cholesterol, with growth only at 12.5 $\mu\text{g}/\text{mL}$. On the other hand, fragment **8** which showed no inhibition of HsaD was also ineffective at concentrations up to 200 $\mu\text{g}/\text{mL}$ in inhibiting the growth of either *M. bovis* BCG or *M. tuberculosis* on cholesterol.

Fragment **2** was capable of inhibiting the growth of *M. bovis* BCG cells with an MIC of <12.5 $\mu\text{g}/\text{mL}$ whilst fragment **24**, inhibit the growth at 25 $\mu\text{g}/\text{mL}$. Fragment **27** on the other hand, did not appear to have an effect, with growth evident even at the highest concentration (200 $\mu\text{g}/\text{mL}$). As with fragment **2**, both fragments **6** and **32**, completely halted growth, with an MIC below 12.5 $\mu\text{g}/\text{mL}$. Isoniazid, gave an MIC of 0.1 mg/mL on bacteria grown on cholesterol.

Similarly, the effect on *M. tuberculosis* growth following treatment with the fragments was also investigated during growth on cholesterol. Treatment with fragments **2** and **6** gave an MIC of 50 $\mu\text{g}/\text{mL}$ and 25 $\mu\text{g}/\text{mL}$ respectively, whilst fragments **24** and **32**, 200 $\mu\text{g}/\text{mL}$. No inhibition was observed with fragments **27** and **8** (growth present at 200 $\mu\text{g}/\text{mL}$) therefore, the MIC could not be calculated. Isoniazid was again found to have an MIC of 0.1 mg/mL.

Fragment **27** is negatively charged and its ineffectiveness in the whole-cell inhibition may possibly be due to a lack of permeation through the lipid-rich mycobacterial cell-wall.

Conclusions

There is growing evidence of the importance of cholesterol for intracellular survival of *M. tuberculosis* and recurring evidence for the importance of the operon encoding HsaD as being essential for intracellular survival of *M. tuberculosis*. We present here evidence based on screening HsaD directly in a fragment based approach, that compounds identified as inhibitors of HsaD also have an effect on growth of *M. tuberculosis* and *M. bovis* BCG on cholesterol. HsaD is being identified as a target through virtual screening and whole cell assays linked with transcriptomic studies are also highlighting the importance of members of this operon. These studies provide a blueprint for extending the search and expanding the inhibitory moieties identified here in the continuing search for a new generation of anti-tubercular agents.

Competing Interests' Statement

None

For Peer Review

References

- Adams PD, Afonine PV, Bunkoczi G, Chen VB, Davis IW, Echols N, *et al.* (2010). PHENIX: a comprehensive Python-based system for macromolecular structure solution. *Acta crystallographica. Section D, Biological crystallography* **66**(Pt 2): 213-221.
- Anderton MC, Bhakta S, Besra GS, Jeavons P, Eltis LD, Sim E (2006). Characterization of the putative operon containing arylamine *N*-acetyltransferase (*nat*) in *Mycobacterium bovis* BCG. *Mol. Microbiol.* **59**(1): 181-192.
- Bardarov S, Bardarov Jr S, Pavelka Jr MS, Sambandamurthy V, Larsen M, Tufariello J, *et al.* (2002). Specialized transduction: an efficient method for generating marked and unmarked targeted gene disruptions in *Mycobacterium tuberculosis*, *M. bovis* BCG and *M. smegmatis*. *Microbiology* **148**(10): 3007-3017.
- Bhakta S, Besra GS, Upton AM, Parish T, Sholto-Douglas-Vernon C, Gibson KJ, *et al.* (2004). Arylamine *N*-acetyltransferase is required for synthesis of mycolic acids and complex lipids in *Mycobacterium bovis* BCG and represents a novel drug target. *The Journal of Experimental Medicine* **199**(9): 1191-1199.
- Blanco FC, Nunez-Garcia J, Garcia-Pelayo, C; Soria, M, Bianco MV, Zumárraga M, Golby P, Cataldi AA, Gordon SV, Bigi F (2009) Differential transcriptome profiles of attenuated and hypervirulent strains of *Mycobacterium bovis* *Microbes and Infection* **11**(12); 956-963.
- Carr H, Purcell E (1954) Effects of diffusion on free precession in nuclear magnetic resonance experiments. *Phys Rev* **94**:630
- Ciulli A (2013). Biophysical screening for the discovery of small-molecule ligands. *Protein-Ligand Interactions: Methods and Applications*: 357-388.
- Ciulli A, Abell C (2007). Fragment-based approaches to enzyme inhibition. *Current opinion in biotechnology* **18**(6): 489-496.
- Collaborative Computational Project (1994). The CCP4 suite: programs for protein crystallography. *Acta crystallographica. Section D, Biological crystallography* **50**(Pt 5): 760-763.
- Crowe AM, Stogios PJ, Casabon I, Evdokimova E, Savchenko A, Eltis LD (2015). Structural and functional characterization of a ketosteroid transcriptional regulator of *Mycobacterium tuberculosis*. *The Journal of biological chemistry* **290**(2): 872-882.
- Dalvit C, Pevarello P, Tatò M, Veronesi M, Vulpetti A, Sundström M. (2000) Identification of compounds with binding affinity to proteins via magnetization transfer from bulk water. *J Biomol NMR* **18**:65–68.

Dalvit C, Fogliatto G, Stewart A, Veronesi M, Stockman B (2001). WaterLOGSY as a method for primary NMR screening: practical aspects and range of applicability. *Journal of biomolecular NMR* **21**(4): 349-359.

Emsley P, Lohkamp B, Scott WG, Cowtan K (2010). Features and development of Coot. *Acta Crystallographica Section D* **66**(4): 486-501.

Evangelopoulos D, Bhakta S (2010). Rapid methods for testing inhibitors of mycobacterial growth. *Antibiotic Resistance Protocols: Second Edition*: 193-201.

Evangelopoulos D, Gupta A, Lack N, Maitra A, ten Bokum AMC, Kendall S L, Sim E, Bhakta S. (2014) Characterisation of a putative *AraC* transcriptional regulator from *Mycobacterium smegmatis*. *Tuberculosis* **94** (6): 664-671.

Evans P (2006). Scaling and assessment of data quality. *Acta crystallographica. Section D, Biological crystallography* **62**(Pt 1): 72-82.

Ferguson FM, Fedorov O, Chaikuad A, Philpott M, Muniz JR, Felletar I, *et al.* (2013). Targeting low-druggability bromodomains: fragment based screening and inhibitor design against the BAZ2B bromodomain. *J. Med. Chem.* **56**(24): 10183-10187.

Griffin JE, Gawronski JD, DeJesus MA, Ioerger TR, Akerley BJ, Sasseti CM. (2011) High-resolution phenotypic profiling defines genes essential for Mycobacterial growth and cholesterol catabolism. *PLoS Pathog* **7**(9): e1002251. doi:10.1371/journal.ppat.1002251

Griffin JE, Pandey AK, Gilmore SA, Mizrahi V, McKinney JD, Bertozzi CR, *et al.* (2012) Cholesterol catabolism by *Mycobacterium tuberculosis* requires transcriptional and metabolic adaptations. *Chem Biol* **19**(2): 218-227.

Hudson SA, McLean KJ, Surade S, Yang YQ, Leys D, Ciulli A, *et al.* (2012). Application of fragment screening and merging to the discovery of inhibitors of the Mycobacterium tuberculosis cytochrome P450 CYP121. *Angewandte Chemie International Edition* **51**(37): 9311-9316.

Hung AW, Silvestre HL, Wen S, George GP, Boland J, Blundell TL, *et al.* (2016). Optimization of Inhibitors of Mycobacterium tuberculosis Pantothenate Synthetase Based on Group Efficiency Analysis. *ChemMedChem* **11**(1): 38-42.

Kabsch W (2010). XDS. *Acta Crystallographica Section D* **66**(2): 125-132.

Kendall SL, Withers M, Soffair CN, Moreland NJ, Gurucha S, Sidders B, *et al.* (2007)

- A highly conserved transcriptional repressor controls a large regulon involved in lipid degradation in *Mycobacterium smegmatis* and *Mycobacterium tuberculosis*. *Mol Microbiol* **65**(3): 684-699.
- Kendall SL, Burgess P, Balhana R, Withers M, ten Bokum A, Lott JS, *et al.* (2010). Cholesterol utilization in mycobacteria is controlled by two TetR-type transcriptional regulators: kstR and kstR2. *Microbiology* **156**(5): 1362-1371.
- Lack N, Lowe ED, Liu J, Eltis LD, Noble ME, Sim E, *et al.* (2008). Structure of HsaD, a steroid-degrading hydrolase, from *Mycobacterium tuberculosis*. *Acta Crystallographica Section F: Structural Biology and Crystallization Communications* **64**(1): 2-7.
- Lack NA, Kawamura A, Fullam E, Laurieri N, Beard S, Russell AJ, *et al.* (2009). Temperature stability of proteins essential for the intracellular survival of *Mycobacterium tuberculosis*. *The Biochemical journal* **418**(2): 369-378.
- Lack NA, Yam KC, Lowe ED, Horsman GP, Owen RL, Sim E, *et al.* (2010). Characterization of a carbon-carbon hydrolase from *Mycobacterium tuberculosis* involved in cholesterol metabolism. *Journal of Biological Chemistry* **285**(1): 434-443.
- Li Q, Ge F, Tan Y, Zhang G, Li W, (2016) Genome-wide transcriptome profiling of *Mycobacterium smegmatis* MC2 155 cultivated in minimal media supplemented with cholesterol, androstenedione or glycerol *Int J Mol Sci* **17** : 689 doi:[10.3390/ijms17050689](https://doi.org/10.3390/ijms17050689)
- Lloyd-Evans E, Lack N, Williams I, Churchill GC, Sim E, Platt FM. (2009) Inhibition of phago-lysosome fusion and foam cell formation by *Mycobacterium bovis* BCG induces a Niemann-Pick type C1 like phenotype. *Chemistry and Physics of Lipids*, **160**,S43–S44. 50th International Conference on the Bioscience of Lipids.
- Lovewell RR, Sasseti CM, VanderVen BC (2016). Chewing the fat: lipid metabolism and homeostasis during *M. tuberculosis* infection. *Current opinion in microbiology* **29**: 30-36.
- McCoy AJ, Grosse-Kunstleve RW, Adams PD, Winn MD, Storoni LC, Read RJ (2007). Phaser crystallographic software. *Journal of applied crystallography* **40**(Pt 4): 658-674.
- McNicholas S, Potterton E, Wilson K, Noble M (2011). Presenting your structures: the CCP4mg molecular-graphics software. *Acta Crystallogr. Sect. D. Biol. Crystallogr.* **67**(4): 386-394.
- Mayer M, Meyer B (1999) Characterization of ligand binding by saturation transfer difference NMR spectroscopy. *Angew Chem Int Ed Engl* **38**:1784–1788.]

Moriarty NW, Grosse-Kunstleve RW, Adams PD (2009). electronic Ligand Builder and Optimization Workbench (eLBOW): a tool for ligand coordinate and restraint generation. *Acta crystallographica. Section D, Biological crystallography* **65**(Pt 10): 1074-1080.

Murshudov GN, Vagin AA, Dodson EJ (1997). Refinement of macromolecular structures by the maximum-likelihood method. *Acta crystallographica. Section D, Biological crystallography* **53**(Pt 3): 240-255.

Niesen FH, Berglund H, Vedadi M (2007). The use of differential scanning fluorimetry to detect ligand interactions that promote protein stability. *Nat. Protoc.* **2**(9): 2212-2221.

Ouellet H, Johnston JB, Montellano PROd (2011). Cholesterol catabolism as a therapeutic target in *Mycobacterium tuberculosis*. *Trends Microbiol.* **19**(11): 530-539.

Pandey AK, Sasseti CM (2008). Mycobacterial persistence requires the utilization of host cholesterol. *Proc. Natl. Acad. Sci. U. S. A.* **105**(11): 4376-4380.

Payton M, Gifford C, Schartau P, Hagemeyer C, Mushtaq A, Lucas S, *et al.* (2001). Evidence towards the role of arylamine N-acetyltransferase in *Mycobacterium smegmatis* and development of a specific antiserum against the homologous enzyme of *Mycobacterium tuberculosis*. *Microbiology* **147**(Pt 12): 3295-3302.

Peyron P, Bordier C, Elsa-Noah N, Maridonneau-Parini I (2000). Nonopsonic phagocytosis of *Mycobacterium kansasii* by human neutrophils depends on cholesterol and is mediated by CR3 associated with glycosylphosphatidylinositol-anchored proteins. *The Journal of Immunology* **165**(9): 5186-5191.

Piotto M, Saudek V, Sklenár V (1992) Gradient-tailored excitation for single-quantum NMR spectroscopy of aqueous solutions. *J Biomol NMR* **2**:661-665..

Rebollo-Lopez MJ, Lelièvre J, Alvarez-, Gomez D, Castro-Pichel J, Martínez-Jiménez F, Papadatos G, Kumar V, Colmenarejo G, Mugumbate G, Hurle M, Barroso V, Young RJ, Martinez-Hoyos M, González del Río R, Bates RH, Lopez-Roman EM, Mendoza-Losana A, Brown JR, Alvarez-Ruiz E, Marti-Renom MA, Overington JP, Cammack, N, Ballell L, Barros-Aguire D. (2015) Release of 50 new, druglike compounds and their computational target predictions for open source anti-tubercular drug discovery. PLoS ONE 10(12): e0142293. doi:10.1371/journal.pone.0142293

Rengarajan J, Bloom BR, Rubin EJ (2005). Genome-wide requirements for *Mycobacterium tuberculosis* adaptation and survival in macrophages. *Proc. Natl. Acad. Sci. U. S. A.* **102**(23): 8327-8332.

Rohde K H., Veiga DFT, Caldwell S, Bala' G, Russell DG. (2012) Linking the transcriptional profiles and the physiological states of *Mycobacterium tuberculosis* during an

extended intracellular infection. *PLoS Pathogens* **8** (6) e1002769.
doi:10.1371/journal.ppat.1002769

Ruzzini AC, Bhowmik S, Ghosh S, Yam KC, Bolin JT, Eltis LD (2013). A Substrate-Assisted Mechanism of Nucleophile Activation in a Ser-His-Asp Containing C-C Bond Hydrolase. *Biochemistry* **52**(42): 7428-7438.

Ruzzini AC, Ghosh S, Horsman GP, Foster LJ, Bolin JT, Eltis LD (2012). Identification of an Acyl-Enzyme Intermediate in a meta-Cleavage Product Hydrolase Reveals the Versatility of the Catalytic Triad. *Journal of the American Chemical Society* **134**(10): 4615-4624.

Ryan A, Keany S, Eleftheriadou O, Ballet R, Cheng H-Y, Sim E (2014). Mechanism-based inhibition of HsaD: a CC bond hydrolase essential for survival of *Mycobacterium tuberculosis* in macrophage. *FEMS microbiology letters* **350**(1): 42-47.

Sassetti CM, Boyd DH, Rubin EJ (2003). Genes required for mycobacterial growth defined by high density mutagenesis. *Mol. Microbiol.* **48**(1): 77-84.

Silvestre HL, Blundell TL, Abell C, Ciulli A (2013). Integrated biophysical approach to fragment screening and validation for fragment-based lead discovery. *Proceedings of the National Academy of Sciences* **110**(32): 12984-12989.

Uhía I, Galán B, Kendall SL, Stoker NG, García JL (2012). Cholesterol metabolism in *Mycobacterium smegmatis*. *Environmental microbiology reports* **4**(2): 168-182.

Van der Geize R, Yam K, Heuser T, Wilbrink MH, Hara H, Anderton MC, *et al.* (2007). A gene cluster encoding cholesterol catabolism in a soil actinomycete provides insight into *Mycobacterium tuberculosis* survival in macrophages. *Proc. Natl. Acad. Sci. U. S. A.* **104**(6): 1947-1952.

VanderVen BC, Fahey RJ, Lee W, Liu Y, Abramovitch RB, *et al.* (2015) Novel inhibitors of cholesterol degradation in *Mycobacterium tuberculosis* reveal how the bacterium's metabolism is constrained by the intracellular environment. *PLoS Pathog* **11**(2): e1004679.
doi: 10.1371/journal.ppat.1004679

Van Molle I, Thomann A, Buckley DL, So EC, Lang S, Crews CM, *et al.* (2012). Dissecting fragment-based lead discovery at the von Hippel-Lindau protein: hypoxia inducible factor 1 α protein-protein interface. *Chemistry & biology* **19**(10): 1300-1312.

Westwood, I., Bhakta, S., Russell, A.,J., Fullam, E., Anderton, M.C., Kawamura, A., Mulvaney, A., Vickers, V.J., Bhowruth, V., Besra, G.S., Lalvani, A., Davies, S.G. & Sim, E. (2010) Identification of arylamine N-acetyltransferase inhibitors as an approach towards novel anti-tuberculars. *Protein & Cell* **1**(1): 82-95

WHO (2015). Global tuberculosis report 2015: http://apps.who.int/iris/bitstream/10665/191102/1/9789241565059_eng.pdf.

Winn MD, Ballard CC, Cowtan KD, Dodson EJ, Emsley P, Evans PR, *et al.* (2011). Overview of the CCP4 suite and current developments. *Acta Crystallographica Section D: Biological Crystallography* **67**(4): 235-242.

Winter G (2010). xia2: an expert system for macromolecular crystallography data reduction. *J. Appl. Crystallogr.* **43**(1): 186-190.

Yam KC, D'Angelo I, Kalscheuer R, Zhu H, Wang JX, Snieckus V, *et al.* (2009). Studies of a ring-cleaving dioxygenase illuminate the role of cholesterol metabolism in the pathogenesis of *Mycobacterium tuberculosis*. *PLoS Path.* **5**(3): e1000344.

Figure Legends

Figure 1. Effect of deletion of *hsaD* gene on *M. bovis* BCG.

Growth rates of Δ *hsaD* and wildtype *M. bovis* BCG in MB7H9 (A) on minimal medium containing 0.05% (v/v) tyloxapol, 0.05% (v/v) ethanol with no additional carbon source (B) or supplemented with, 100 μ g/mL cholesterol (C) or 100 μ g/mL glycerol (D). The intracellular survival of Δ *hsaD* *M. bovis* BCG relative to the wild-type in RAW264.7 cells (E) was determined as described in Methods. The mean \pm standard deviation of three values is shown.

Figure 2 Identification of fragment inhibitors of HsaD

(A) NMR screening of DSF hits. Water-suppressed 1D 1 H and STN NMR screening spectra for a representative fragment hit (fragment 2, at 1.2 mM) in the presence and absence of HsaD (10 μ M) plus PMSF (100 μ M). Only the fragment resonances in the aromatic region of the spectra are shown. The strong positive fragment signals in the presence of HsaD (purple spectrum) indicate binding, and this interaction is reduced by the addition of PMSF. (B) Inhibition of HsaD by DSF hits confirmed by NMR. Fragments identified by DSF as binding to HsaD were assayed for inhibition as described in materials and methods at 1 mM (filled bars). The mean of triplicate \pm standard deviation is shown. Fragments are numbered as shown in Table 1. 100% activity was defined as the rate of enzymatic HOPDA hydrolysis by 16 μ g/mL HsaD with vehicle (no compound), which was 0.08 μ mol/min/(mg protein).

Figure 3. Binding of inhibitors to HsaD.

(A) The active site residues of apo HsaD (Lack *et al.*, 2008) are overlaid onto the active site residues of HsaD bound to fragment 27 (fragment not shown). (B) Fragment 2, (C) Fragment 27 and (D) Fragment 32 each bound to HsaD. In (A) HsaD structure with compound 2 has blue carbon atoms, apo-HsaD has gold carbon atoms. In (B) - (D) Green mesh is unbiased positive difference density contoured at 3σ . In (B) - (D) the protein is shown with blue carbon atoms, 2 is shown with grey carbon atoms, 27 with brown carbon atoms and 32 with cyan carbon atoms. Chlorines are coloured pink and hydrogen bonds are black dashed lines. Interacting residues are labelled. All figures were generated in CCP4MG (McNicholas *et al.*, 2011).

Figure 4. Comparison of the orientation of binding of fragments to the HsaD active site.

(A) Shows the overlaid binding orientations of compounds 27 and 32. (B) shows the overlaid binding orientations of compounds 2 and 27. (C) shows the electrostatic potential surface map of HsaD in the pocket around compound 2. (D) shows an overlay of the structure of

HsaD bound to **2** with the structure of HsaD bound to HOPDA (PDB code 2wug) (Lack *et al.*, 2010). Colour coding of carbon atoms is as per figure 3. HOPDA is shown with purple carbon atoms. CCP4MG was used to perform secondary structure alignments for as well as generating the electrostatic potential maps for (C) and (D).

Supplementary Figure legends

Supplementary figure 1:

Cultures of *Mycobacterium smegmatis* grown on minimal medium containing cholesterol as carbon source are coloured when HsaD is deleted. Wildtype (WT) – on the left and $\Delta HsaD$ on the right. *Mycobacterium smegmatis* were grown in 7H9 (containing 50µg/ml hygromycin for knockout) to an OD=1, washed twice with sterile PBS and then used to inoculate (1/100 dilution) a 200mL culture of minimal medium containing 0.05% (v/v) ethanol, 0.05% (v/v) tyloxapol and 50µg/ml cholesterol and grown at 37°C for 36 hours.

Supplementary figure 2.

Effect of fragments on the growth of *E. coli* JM109 in LB medium

(A) fragment **2**; (B) fragment **24**; (C) fragment **27**; (D) fragment **32**; and (E) fragment **6**. Liquid cultures in LB were diluted to an OD₆₀₀ of 0.1 and fragments were added. Briefly, an overnight culture was sub-cultured and was diluted to an OD₆₀₀ of 0.1 in LB containing 12.5 µg/mL, 25 µg/mL, 50µg/mL, or 100 µg/mL of fragments. Absorbance readings at 600nm represent means of triplicates ± S.D.

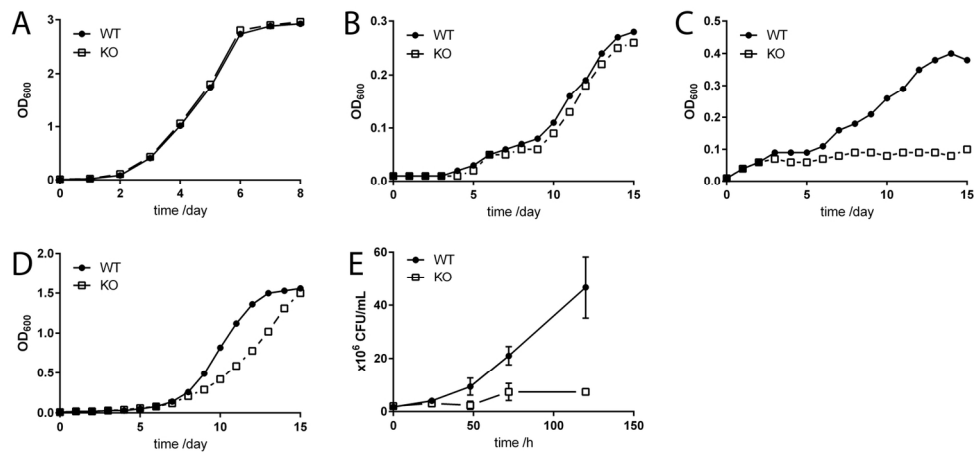
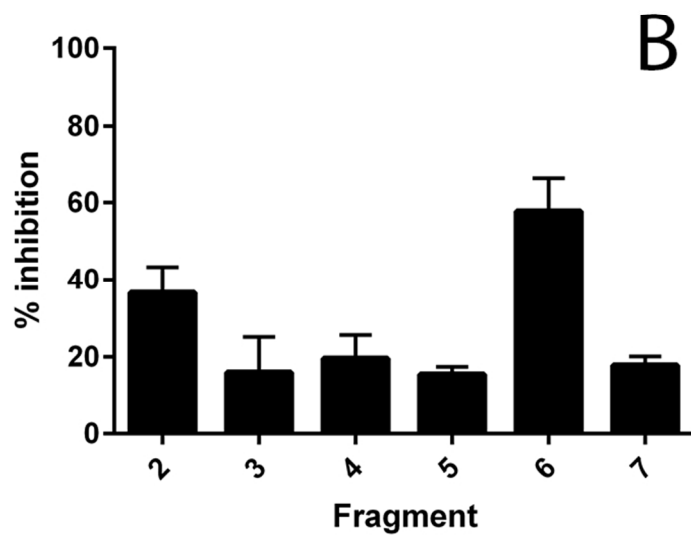
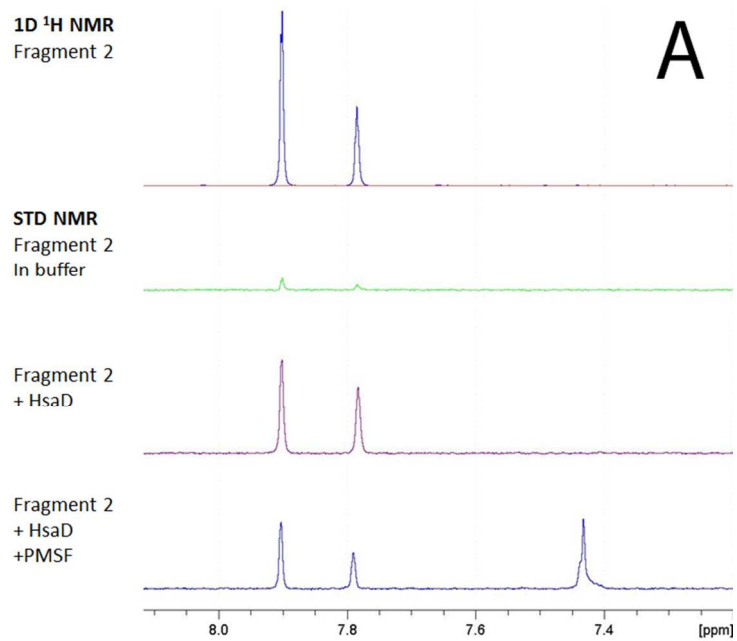


Figure 1. Effect of deletion of *hsaD* gene on *M. bovis* BCG. Growth rates of Δ *hsaD* and wildtype *M. bovis* BCG in MB7H9 (A) on minimal medium containing 0.05% (v/v) tyloxapol, 0.05% (v/v) ethanol with no additional carbon source (B) or supplemented with , 100 μ g/mL cholesterol (C) or 100 μ g/mL glycerol (D). The intracellular survival of Δ *hsaD* *M. bovis* BCG relative to the wild-type in RAW264.7 cells (E) was determined as described in Methods. The mean \pm standard deviation of three values is shown. 148x69mm (300 x 300 DPI)



60x99mm (300 x 300 DPI)

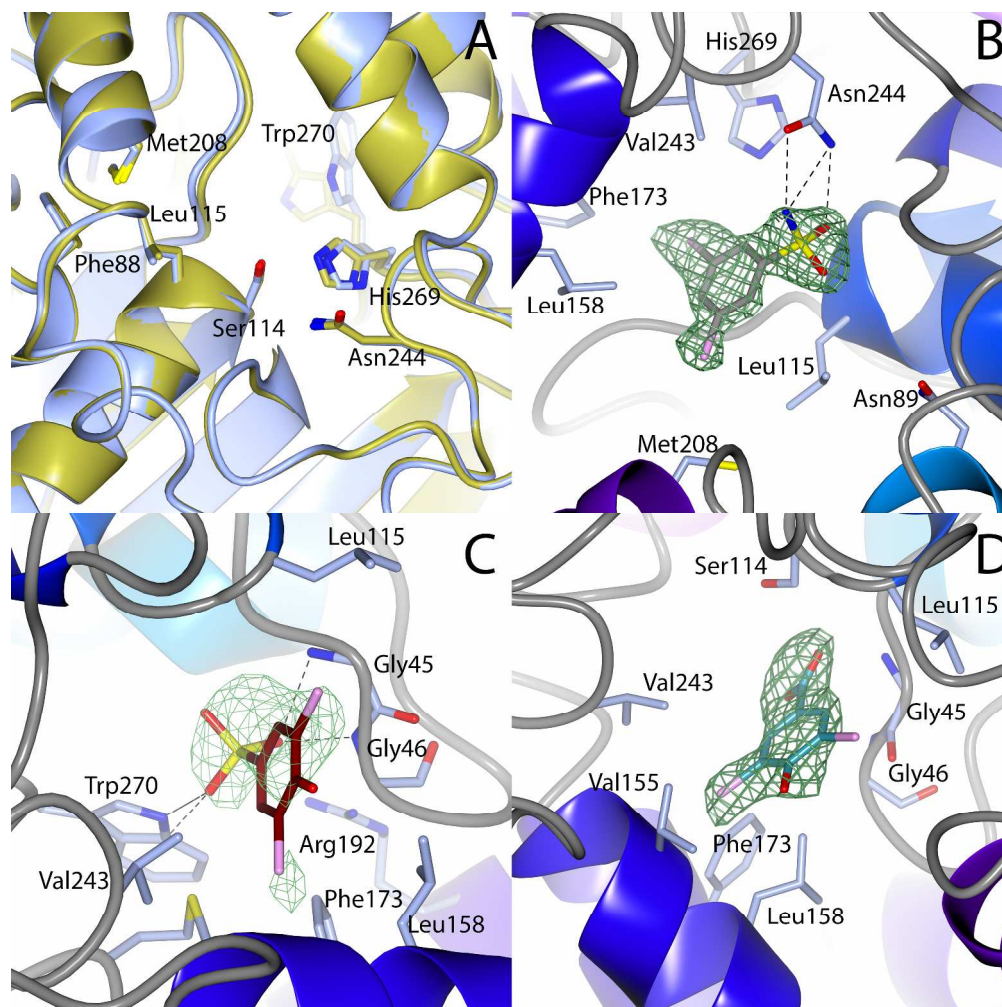


Figure 3. Binding of inhibitors to HsaD. (A) The active site residues of apo HsaD (Lack et al., 2008) are overlaid onto the active site residues of HsaD bound to fragment 2 (fragment not shown). (B) Fragment 2, (C) Fragment 27 and (D) Fragment 32 each bound to HsaD. In (A) HsaD structure with compound 2 has blue carbon atoms, apo-HsaD has gold carbon atoms. In (B) - (D) Green mesh is unbiased positive difference density contoured at 3σ . In (B) - (D) the protein is shown with blue carbon atoms, 2 is shown with grey carbon atoms, 27 with brown carbon atoms and 32 with cyan carbon atoms. Chlorines are coloured pink and hydrogen bonds are black dashed lines. Interacting residues are labelled. All figures were generated in CCP4MG (McNicholas et al., 2011).

304x304mm (300 x 300 DPI)

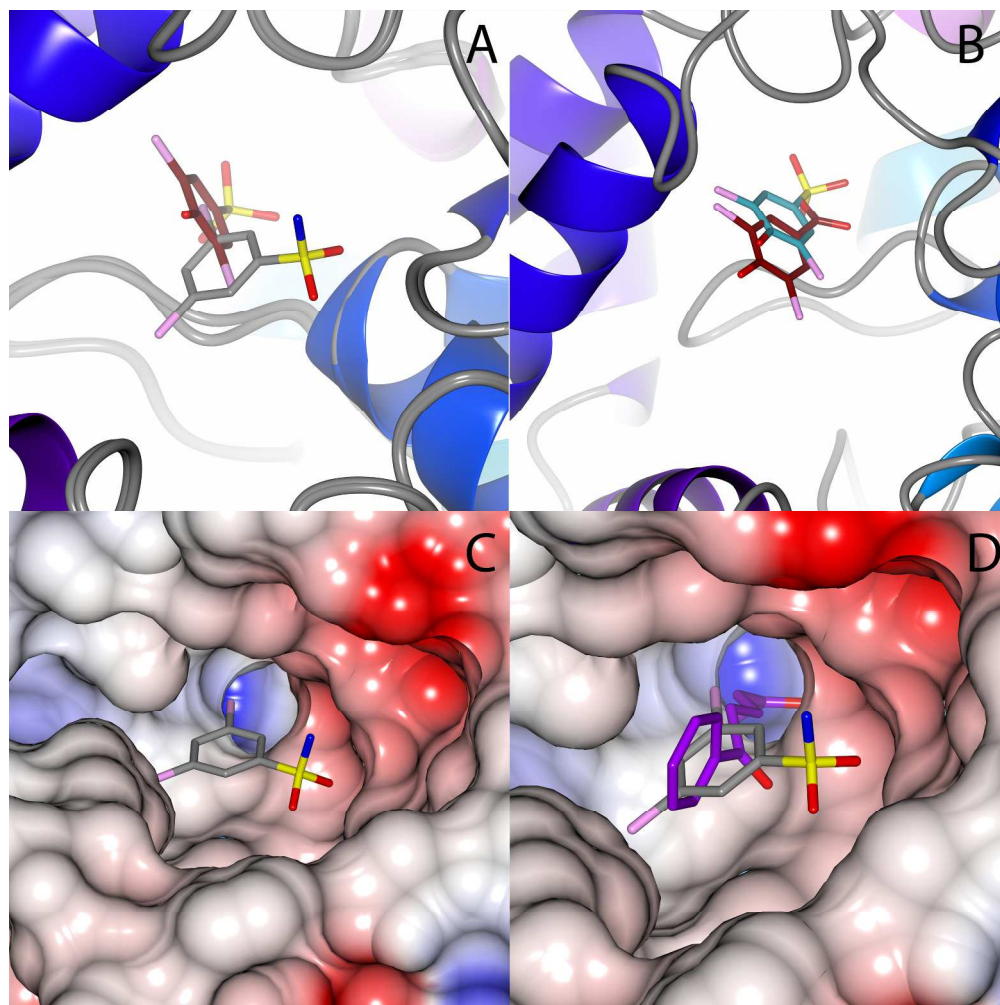


Figure 4. Comparison of the orientation of binding of fragments to the HsaD active site. (A) Shows the overlaid binding orientations of compounds 27 and 32. (B) shows the overlaid binding orientations of compounds 2 and 27. (C) shows the electrostatic potential surface map of HsaD in the pocket around compound 2. (D) shows an overlay of the structure of HsaD bound to 2 with the structure of HsaD bound to HOPDA (PDB code 2wug) (Lack et al., 2010). Colour coding of carbon atoms is as per figure 3. HOPDA is shown with purple carbon atoms. CCP4MG was used to perform secondary structure alignments for as well as generating the electrostatic potential maps for (C) and (D).

254x254mm (300 x 300 DPI)

Table 1

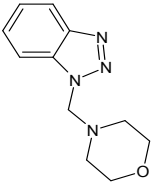
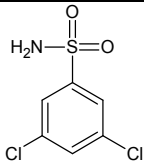
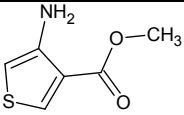
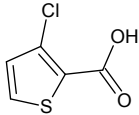
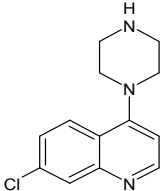
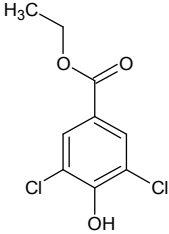
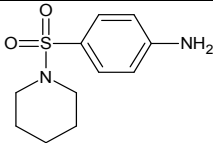
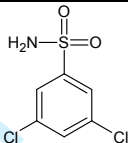
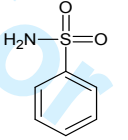
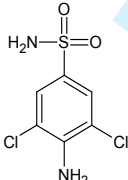
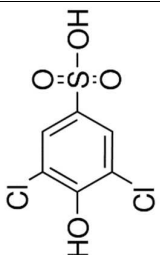
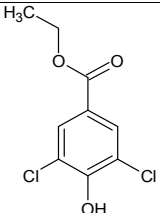
| Compound | T _M shifts* | NMR | PMSF displacement | Structure |
|----------|---------------------------|-----|-----------------------------------|---|
| 1 | 1.78; 2.64; 2.64 | Hit | Displaced |  |
| 2 | 0.77; 0.38; 0.38 | Hit | Displaced |  |
| 3 | 0.55; 0.76; 0.76 | Hit | Displaced |  |
| 4 | 0.55; -2.26; -2.26 | Hit | Displaced |  |
| 5 | 0.92; 1.13; 1.13 | Hit | Not displaced (PMSF bound) |  |
| 6 | 0.70; 1.13; 1.13 | Hit | Not displaced (PMSF not bound) |  |
| 7 | 0.82; 0.38; 0.76 | Hit | Displaced |  |

Table 1. Fragments from a 1258 member library producing a significant shift in HsaD T_M and where saturation NMR demonstrated displacement of the ligand by PMSF.

The compounds are numbered sequentially : 4-((1H-benzo[d][1,2,3] triazol-1-yl)methyl)morpholine compound 1; 3,5,-dichloro-benzenesulfonamide compound 2; methyl 4-aminothiophene-3-carboxylate compound 3; 3-chlorothiophene-2-carboxylic acid , compound 4; 7-chloro-4-(piperazin-1-yl)quinolone, compound 5; ethyl 3,5-dichloro-4-hydroxybenzoate, compound 6; 4-(piperidin-1-ylsulfonyl)aniline, compound 7.

*The T_M shifts are shown for each compound tested with a positive result for DSF, performed as described in materials and methods at 2.5 mM final fragment concentration per well. Structures are drawn with ChemDraw Ultra 12.0 (CambridgeSoft). Hits from the primary DSF screen were re-tested twice to confirm results of the initial screen and finally validated for protein binding using NMR spectroscopy (as shown in Fig. 2A) (after Ciulli & Abell, 2007; Mayer & Meyer, 1999).

| ID | Compound | Structure | IC ₅₀ (mM) | MIC (µg/mL) Growth on cholesterol | |
|----|---|---|--------------------------|--------------------------------------|------------------------|
| | | | | <i>M. bovis</i> BCG | <i>M. tuberculosis</i> |
| 2 | 3,5,-dichloro-benzenesulfonamide |  | 0.43 ±0.03 | <12.5 | 25 |
| 8 | Benzenesulfonamide |  | NI | NI | NI |
| 24 | 3,5-dichlorosulfanilamide |  | 0.18±0.0 1 | 25 | 200 |
| 27 | 3,5-dichloro-4-hydroxybenzenesulphonic acid |  | 0.27 ±0.03 | >200 | >200 |
| 6 | ethyl 3,5-dichloro-4-hydroxybenzoate |  | 0.55±0.0 7 | <12.5 | <12.5 |

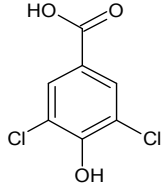
| | | | | | |
|----|------------------------------------|---|---------------|-------|-----|
| 32 | 3,5-dichloro-4-hydroxybenzoic acid |  | 0.54 ±0.01 | <12.5 | 200 |
|----|------------------------------------|---|---------------|-------|-----|

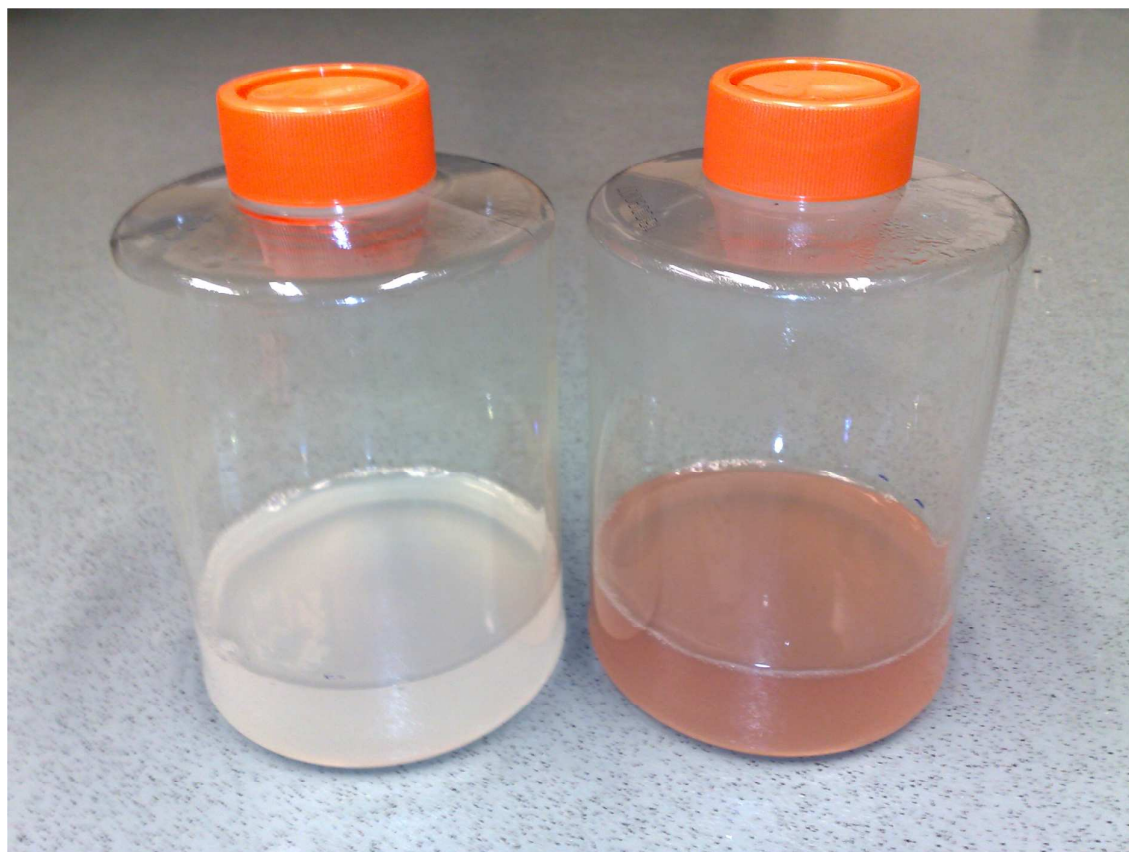
Table 2 Effects of (A) Fragment 2 and its derivatives and (B) fragment 6 and a derivative on HsaD enzymic activity and growth of mycobacteria on cholesterol as carbon source.

NI indicates no inhibition observed at 5mM for inhibition of enzyme activity and no inhibition of growth at 200 µg/mL as described in Methods.

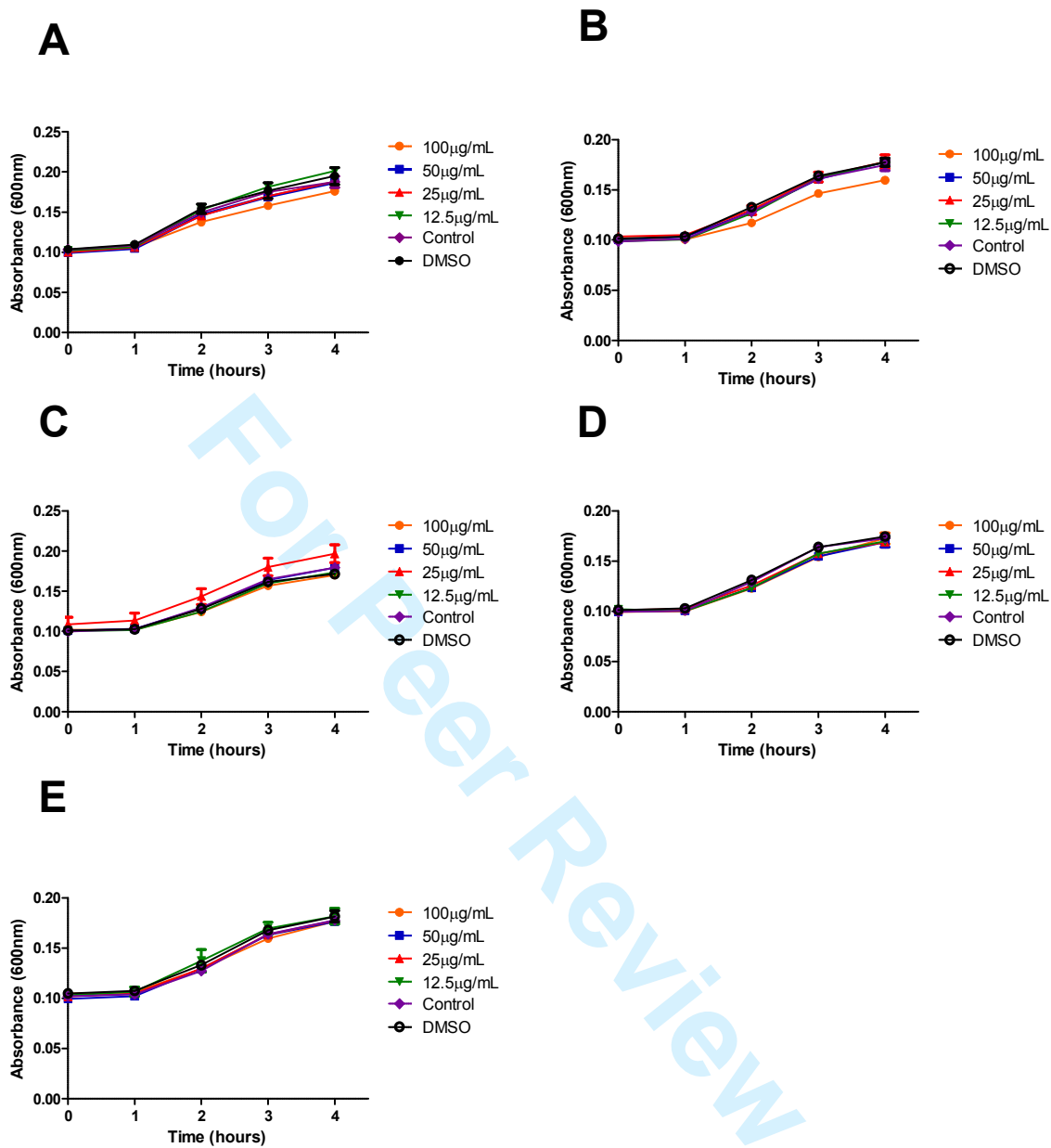
See supplementary table 1 for full list.

Table 3 Processing and refinement statistics for X-ray crystallographic structures.

| Structure | HsaD - 2 | HsaD - 27 | HsaD - 32 |
|---|--|--|--|
| PDB Code | 5JZB | 5JZ9 | 5JZS |
| Space Group | I 2 ₁ 2 ₁ 2 ₁ | I 2 ₁ 2 ₁ 2 ₁ | I 2 ₁ 2 ₁ 2 ₁ |
| α, β, γ (°) | 90, 90, 90 | 90, 90, 90 | 90, 90, 90 |
| a, b, c (Å) | 82.03, 82.23, 194.25 | 81.73, 82.32, 193.58 | 81.92, 82.27, 195.13 |
| Processing Statistics | | | |
| Resolution Range (Å) | 50.9-2.1 | 75.75-2.68 | 97.57-2.27 |
| Unique reflections ^a | 38,700 | 18,699 (2,445) | 30,015 (2,024) |
| R_{merge} | 0.134 (0.469) | 0.231 (0.895) | 0.109 (0.453) |
| $\langle I/\sigma(I) \rangle^a$ | 8 (2.6) | 4.4 (1.5) | 7.7 (1.4) |
| Completeness % ^a | 100 (100) | 99.6 (99.0) | 99.3 (57.4) |
| Multiplicity ^a | 6.3 (5.3) | 4.4 (4.5) | 4.9 (3.1) |
| Refinement Statistics | | | |
| R_{work} % | 23.51 | 24.05 | 23.48 |
| R_{free} % | 20.55 | 21.27 | 20.25 |
| RMS bond angle (°) | 1.28 | 0.89 | 1.20 |
| RMS bond length (Å) | 0.005 | 0.004 | 0.009 |
| Ramachandran Statistics^b | | | |
| Preferred region % | 97.5 | 98.2 | 98.6 |
| Allowed region % | 2.3 | 1.8 | 1.4 |
| Outliers % | 0.2 | 0 | 0 |
| ^a Numbers in parentheses are for the highest resolution shell. | | | |
| ^b Ramachandran statistics were calculated using MolProbity. | | | |



Supplementary Figure 1: Cultures of *Mycobacterium smegmatis* grown on minimal medium containing cholesterol as carbon source are coloured when HsaD is deleted. Wildtype (WT) – on the left and $\Delta HsaD$ on the right *Mycobacterium smegmatis* were grown in 7H9 (containing 50 μ g/ml hygromycin for knockout) to an OD=1, washed twice with sterile PBS and then used to inoculate (1/100 dilution) a 200mL culture of minimal medium containing 0.05% (v:v) EtOH, 0.05% (v:v) tyloxapol and 50 μ g/ml cholesterol and grown at 37°C for 36 hours.



Supplementary figure 2: Effect of fragments on the growth of *E. coli* JM109 in LB medium (A) fragment 2; (B) fragment 24; (C) fragment 27; (D) fragment 32; and (E) fragment 6. Liquid cultures in LB were diluted to an OD₆₀₀ of 0.1 and fragments were added Briefly, an overnight culture was sub-cultured and was diluted to an OD₆₀₀ of 0.1 in LB containing 12.5 µg/mL, 25 µg/mL, 50 µg/mL, or 100 µg/mL of fragments. Absorbance readings at 600nm represent means of triplicates ± S.D.

| Fragment | Fragment name | IC ₅₀ /mM |
|----------|--|----------------------|
| 1 | 4-((1H-benzo[d][1,2,3] triazol-1-yl)methyl) morpholine | ND |
| 2 | 3,5,-dichloro-benzenesulfonamide | 0.43 ±0.03 |
| 3 | methyl 4-aminothiophene-3-carboxylate | * |
| 4 | 3-chlorothiophene-2-carboxylic acid | * |
| 5 | 7-chloro-4-(piperazin-1-yl)quinolone | * |
| 6 | ethyl 3,5-dichloro-4-hydroxybenzoate | 0.55±0.07 |
| 7 | 4-(piperidin-1-ylsulfonyl)aniline | * |
| 8 | Benzenesulfonamide | no inhibition |
| 9 | 3-chlorobenzenesulfonamide | 5.14 ±0.6 |
| 10 | 3,5-difluorobenzenesulfonamide | no inhibition |
| 11 | 2,5-dichlorobenzenesulfonamide | 1.96 ±0.12 |
| 12 | 3,5-bis(trifluoromethyl) benzenesulphonamide | ND |
| 13 | 4-chlorobenzenesulfonamide | no inhibition |
| 14 | 3-bromobenzenesulfonamide | 2.74 ±0.31 |
| 15 | 4-sulfamoylbenzoic acid | no inhibition |
| 16 | 3-nitrobenzenesulfonamide | * |
| 17 | 4-nitrobenzenesulfonamide | no inhibition |
| 18 | 3-aminobenzenesulfonamide | no inhibition |
| 19 | p-aminobenzenesulfonamide | No inhibition |
| 20 | 3-methoxybenzenesulfonamide | * |
| 21 | 4-methoxybenzenesulfonamide | * |
| 22 | 4-hydroxybenzenesulfonamide | no inhibition |
| 23 | p-toluenesulfonamide | no inhibition |
| 24 | 3,5-dichlorosulfanilamide | 0.18 ±0.01 |
| 25 | 2,5-dichloro-N,N-dimethylsulanilamide | 3.63 ±0.24 |
| 26 | 3,5-dibromosulfanilamide | 2.16 ±0.15 |
| 27 | 3,5-dichloro-4-hydroxybenzenesulphonate | 0.27 ±0.03 |
| 28 | 3,5-dichlorobenzoate | no inhibition |
| 29 | 3-chloro-4-hydroxybenzoate | no inhibition |
| 30 | p-hydroxy benzoate | no inhibition |
| 31 | methyl 3,5-dichloro-4-hydroxybenzoate | 0.73 ±0.03 |
| 32 | 3,5-dichloro-4-hydroxybenzoate | 0.54 ±0.01 |
| 33 | 4-amino-3,5-dichlorobenzoate | 0.54 ±0.02 |

| | | |
|----|-----------------------------|---------------|
| 34 | 3,5-dichlorobenzamide | * |
| 35 | 1,3-dichloro-6-nitrobenzene | 2.14 ±0.21 |
| 36 | 4-amino benzoic acid | * |
| 37 | m-aminobenzoic acid | no inhibition |

Table 1 Supplementary Inhibition of HsaD enzymic activity by a sublibrary of compounds based on fragments 2 and 6 from the initial screen (Table 1).

The values for IC₅₀ were determined from the inhibition of HsaD enzymic activity by the fragments as indicated in Materials and Methods. The values shown are averages +/- standard deviation of three independent determinations. No inhibition indicates that the compounds were not inhibitory at 5mM or at the highest soluble concentration which could be obtained. The * indicates that inhibition was observed but that it did not reach 50% at either 5mM or the highest soluble concentration which could be obtained.